RSC Advances

PAPER

View Article Online
View Journal | View Issue

Cite this: *RSC Adv.*, 2019, **9**, 721

Preparation and visible-light photocatalytic properties of the floating hollow glass microspheres – TiO_2/Ag_3PO_4 composites†

Yu An, [a] Pengwu Zheng*[b] and Xiaofei Ma*[ac]

A novel floating visible-light photocatalyst (HGMs–TiO_2/Ag_3PO_4) composite was prepared using amino modified low-density hollow glass microspheres (HGMs) as carriers to disperse and support TiO_2 and Ag_3PO_4 photocatalysts. The surface morphology, crystal structure and optical properties of the HGMs–TiO_2/Ag_3PO_4 composites were characterized and the Ag_3PO_4 content on the surface of the microspheres was determined by atomic absorption spectrometry (AAS). Methylene blue (MB) was chose as the organic pollutant to investigate the visible-light catalytic properties of the HGMs–TiO_2/Ag_3PO_4 composites. For HGM composite photocatalysts, when the theoretical mass ratio of TiO_2 to Ag_3PO_4 on the surface of HGMs is 1 : 1.5, the visible-light catalytic activity of the composite is superior to pure Ag_3PO_4 and a TiO_2/Ag_3PO_4 photocatalyst with a mass ratio of 1 : 1.5 under the same conditions, due to the increased light-contact area and the photocatalytic active sites, since the TiO_2 and Ag_3PO_4 particles can be well dispersed on the surface of the floating HGMs. Furthermore, the deposits of TiO_2 and Ag_3PO_4 on the HGM surface form a heterostructure, facilitating the separation of electron–hole (e^- – h^+) in the energy band, and elevating the photocatalytic activity and cycle stability of Ag_3PO_4. This work indicates that floating HGMs–TiO_2/Ag_3PO_4 composites could become a promising photocatalyst for organic dye removal due to the low cost and high visible-light responsiveness.

Received 20th October 2018
Accepted 19th December 2018

DOI: 10.1039/c8ra08697d

rsc.li/rsc-advances

1. Introduction

With the development of industrialization, the issues of energy shortage and environmental pollution have become increasingly severe. Solar energy, the most abundant clean energy, hitting the earth within one hour is higher than the energy consumed by humans throughout the year.[1] Using renewable solar energy, photocatalytic technology that undergoes redox reactions is a sustainable method to solve environmental problems, especially removing residual dye contaminants in wastewater.

Since Fujishima and Honda used TiO_2 electrodes for photocatalytic decomposition of water under ultraviolet light for the first time in 1972, significant advances have been made in the design of *Z*-scheme photocathodes[2] and research on high-efficiency semiconductor photocatalysts.[3–9] In recent years, various types of semiconductor photocatalysts, such as $In(OH)_3$,[10] $BiVO_4$,[11] ZnO,[12] CdS,[13,14] CuO,[15] Cu_2O,[16] Fe_2O_3,[17] AgBr,[18] Ag_3PO_4,[19] g-C_3N_4,[20] MOF[21] have been reported. TiO_2 is one of the most widely used photocatalytic materials in a wide range of semiconductors due to its high chemical inertness, corrosion resistance, non-toxicity, cost effectiveness, and environmental friendliness. However, owing to its wide bandgap (3.0–3.2 eV), TiO_2 can only absorb ultraviolet light that accounts for 4% of the total sunlight, which greatly limits its practical application under visible light.[4,22] Therefore, the study of visible light-driven high-efficiency photocatalysts has become a hot issue in the field of semiconductor photocatalysis.

During the past few decades, Ag-based photocatalysts have been developed as high-efficiency photocatalysts to degrade organic contaminants such as AgX (X = Cl, Br, and I),[18,23,24] Ag_2O,[25] and Ag_2CO_3.[26] In 2010, Yi *et al.*[27] reported the new use of Ag_3PO_4 in the photooxidation of water and degradation of organic dyes under visible light. The indirect band gap of Ag_3PO_4 is 2.36 eV, and the direct bandgap is 2.43 eV. Both the large dispersion of the conduction band and the strong inducing effect of PO_4^{3-} promote the separation of the photogenerated electron–hole pairs (e^- – h^+) of the Ag_3PO_4, making it one of the currently promising visible-light catalysts.[28] However, Ag_3PO_4 will undergo photo-corrosion to produce Ag particles that affect its photocatalytic activity.[29–31] Therefore, it is critical to develop a novel Ag_3PO_4-based visible-light photocatalyst with improved photocatalytic activity and stability.

[a]*Chemistry Department, School of Science, Tianjin University, Tianjin 300072, PR China. E-mail: maxiaofei@tju.edu.cn; Fax: +86 22 27403475; Tel: +86 22 27406144*
[b]*School of Pharmacy, Jiangxi Science and Technology Normal University, Nanchang, Jiangxi 330013, PR China. E-mail: zhengpw@126.com*
[c]*National Demonstration Center for Experimental Chemistry & Chemical Engineering Education, Tianjin University, Tianjin 300354, China*

† Electronic supplementary information (ESI) available. See DOI: 10.1039/c8ra08697d

In this paper, low-density hollow glass microspheres (HGMs) were used as carriers, and TiO_2 was loaded on the surface of HGMs by hydrothermal method at first, and then floating HGMs–TiO_2/Ag_3PO_4 composites were prepared by ion exchange method with Ag_3PO_4. The as-prepared floating photocatalyst enlarge the contact area between the photocatalyst and light on the one hand, and on the other hand, both the synergistic effect of TiO_2 and Ag_3PO_4 semiconductor and the formation of surface heterojunction can promote the e^-–h^+ charge separation, thus the photocatalytic activity and stability of the photocatalyst is further enhanced.

2. Experimental

2.1. Materials

HGMs (density $\rho = 0.26$ g cm^{-3}) were obtained from Zhengzhou Hollowhite Corp (Henan, China). (3-Aminopropyl)triethoxysilane (APTES) was purchased from Shanghai Aladdin Chemistry Corp (China). All of the other reagents were analytical grade and purchased from Tianjin Chemical Company (China).

2.2. Preparation of amino modified HGMs

10 g of HGMs were added into 50 mL of deionized water in which 40 μL APTES was dissolved under stirring. The floating product (aminated modified HGMs) was washed several times with distilled water and absolute ethanol and dried at 60 °C for 8 h.

2.3. Fabrication of HGMs–TiO_2 composite

2 g amino modified HGMs was dispersed in the mixed solution of 1.28 mL titanium butoxide ($Ti(OC_4H_9)_4$) and 20 mL absolute ethanol with stirring. Then, 40 mL 50% ethanol–water solution was added to the above HGMs suspension through a constant pressure dropping funnel. The mixture was transferred into a 100 mL Teflon-lined stainless-steel autoclave and heated at 120 °C for 5 h. After cooling down to the room temperature, the obtained floating product was washed with distilled water and ethanol for three times and dried at 60 °C for 8 h. The sample was placed in a muffle furnace at 300 °C for 2 h, and taken out after the furnace chamber temperature was lowered to 60 °C. The theoretical TiO_2 loading of the obtained sample was 0.15 g g^{-1} HGMs, labeled as HGMs-1 : 0. At the same time, the same method was used to prepare pure TiO_2 powder without adding HGMs.

2.4. Preparation of HGMs–TiO_2/Ag_3PO_4 composite

1.15 g HGMs-1 : 0 was dispersed in 100 mL $AgNO_3$ solution and stirred for 5 h. Then, 100 mL Na_3PO_4 solution was slowly added dropwise to the above mixture solution and stirred for 30 min. The obtained floating product was washed with distilled water to remove unreacted ions and dried at 60 °C for 8 h. HGMs–TiO_2/Ag_3PO_4 composites with different theoretical loadings of Ag_3PO_4 (0.150, 0.225 and 0.300 g g^{-1} HGMs) were prepared by adjusting the concentration of $AgNO_3$ and Na_3PO_4 aqueous solution and maintaining the stoichiometry of $AgNO_3$ and Na_3PO_4 to 3 : 1. According to the theoretical loading mass ratio of TiO_2 and Ag_3PO_4, the obtained samples were labeled as HGMs-1 : 1, HGMs-1 : 1.5 and HGMs-1 : 2, respectively. At the same time, pure Ag_3PO_4 was prepared without adding HGMs-1 : 0, and TiO_2/Ag_3PO_4 composite with mass ratio of 1 : 1.5 was synthesized by the same preparation method as HGMs–TiO_2/Ag_3PO_4 without adding HGMs.

The fabrication process of the photocatalyst was exhibited in Fig. 1.

2.5. Characterization

The morphology of HGMs–TiO_2/Ag_3PO_4 composite fixed on the sample holder with conducting resin and subjected to gold spray treatment was observed with a Hitachi S-4800 scanning electron microscope. The qualitative analysis of the elemental distribution on the surface of obtained composites was determined by energy dispersive spectrometer (EDS) in conjunction with SEM at an accelerating voltage of 3 kV. The X-ray diffraction (XRD) patterns of photocatalyst composites were recorded in reflection mode in the range of 10–80° (2θ) at a scanning rate of 0.067° s^{-1} with a D/MAX-2500 operated at a CuKα wavelength of 1.542 Å. The ultraviolet-visible diffuse reflectance spectra (DRS) were characterized with UV-2450 spectrophotometer in the range of 200 to 800 nm by using $BaSO_4$ as the reflectance standard material, and measured by the standard Kubelka–

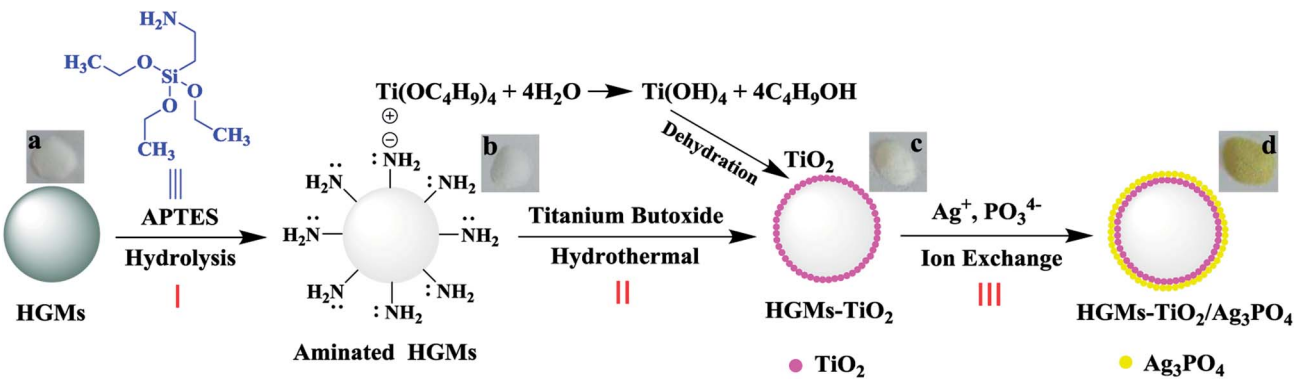

Fig. 1 Schematic illustration of the fabrication process of floating HGMs–TiO_2/Ag_3PO_4 composite. (Inset: digital photos of HGMs (a), aminated HGMs (b), HGMs–TiO_2 (c) and HGMs–TiO_2/Ag_3PO_4 (d)).

Munk method. When Ag_3PO_4 on HGMs–TiO_2/Ag_3PO_4 composites were dissolved with 1 : 1 (v/v) dilute nitric acid solution, the Ag_3PO_4 loadings were calculated by testing the Ag^+ contents by Thermo Scientific iCE3000 atomic absorption spectroscopy (AAS) using a silver lamp as a hollow cathode lamp.

2.6. Photocatalytic activity testing

The photocatalytic property of HGMs–TiO_2/Ag_3PO_4 composites was evaluated by organic dye methylene blue (MB) as the target of photodegradation under simulated sunlight. 0.12 g obtained photocatalyst was dispersed in 60 mL 5 mg L^{-1} MB solution. Before the photocatalytic test began, the photocatalyst was stored in the dark for 60 min to reach adsorption–desorption equilibrium. Then, the photocatalyst-containing MB solution was vertically irradiated with a 300 W xenon lamp and the illumination intensity was 140 mW cm^{-2} from wavelength ranges of 400 to 600 nm. In order to simulate the degradation of dye contaminants in the natural state, magnetic stirring is not performed during the entire photodegradation of MB solution. The liquid level of MB solution in all test was 9.5 cm away from the light source and the depth of the solution was 11.5 cm. At a time interval of 5 min, 3 mL suspension was pipetted with a disposable syringe, then filtered through 0.22 μm millipore membrane filter to remove the photocatalyst particles. The concentration of MB solution was determined by Mapada UV-1800 spectrophotometer at the maximum absorption wavelength of MB (663 nm) with distilled water as reference solution.

The photocatalytic stability and recyclability of the composites were evaluated by the cycling degradation experiments of the 5 mg L^{-1} MB solution. At the end of each cycle, the floating composite was separated and dried at 60 °C for 4 h.

3. Results and discussion

3.1. Synthesis process of HGMs–TiO_2/Ag_3PO_4 photocatalysts

Fig. 1 depicted the fabrication process of HGMs–TiO_2/Ag_3PO_4 composites. The first I step was the amino modification of HGMs. HGMs were modified by the hydrolysis of silane coupling agent APTES to introduce –NH_2 groups on HGMs. Aminated HGMs (Fig. 1b) look the same as raw materials HGMs (Fig. 1a) and are all white powder. The second II step was to prepare HGMs–TiO_2 from aminated HGMs by hydrothermal synthesis. The outer electron arrangement of Ti^{4+} in titanium butoxide ($Ti(OC_4H_9)_4$) was $1s^22s^22p^63s^23p^6$, and the 3d orbital was completely empty. The nitrogen atom in –NH_2 of aminated HGMs had the lone pair electrons that can be filled in its empty 3d orbit and the positively charged Ti^{4+} was adsorbed to the surface of aminated HGMs by electrostatic interaction. With the hydrothermal reaction of $Ti(OC_4H_9)_4$ and the dehydration of intermediates $Ti(OH)_4$, TiO_2 was loaded onto the surface of the HGMs. The obtained HGMs–TiO_2 was also white powder (Fig. 1c). The third III step was to prepare HGMs–TiO_2/Ag_3PO_4 by ion reaction ($Ag^+ + PO_4^{3-} = Ag_3PO_4$) on the surface of HGMs–TiO_2. TiO_2 is an amphoteric oxide with super-hydrophilicity, and its surface easily adsorbs water to form hydroxyl groups. When HGMs–TiO_2 was dispersed in Ag^+ solution, the main species on the surface of the TiO_2 particles was negatively charged O^- anion,[32] which can adsorb positively charged Ag^+ by electrostatic attraction. With Ag^+ adsorbed, the reaction of Ag^+ and PO_4^{3-} took place on the surface of TiO_2 and the color of the floating HGMs–TiO_2 gradually changed from the initial white to yellow (Fig. 1d), indicating the formation of Ag_3PO_4/TiO_2 heterostructure onto HGMs.

3.2. Characterization of the composites

The morphologies of the composites were observed in Fig. 2. HGMs–TiO_2 (Fig. 2a and b) had an uneven surface compared to the originally smooth HGMs (inset in Fig. 2a). From the higher magnification of Fig. 2b, it can be clearly seen that the surface of the HGMs was coated with a layer of TiO_2 particles. These indicated that TiO_2 was successfully coated on the HGMs. And Fig. 2c showed the HGMs-1 : 1.5 was coated with more particles than Fig. 2b, and was enlarged to 500 nm as shown in Fig. 2d with an average particle size less than 50 nm (similar SEM images of HGMs-1 : 1 and HGMs-1 : 2 in Fig. S1†). Fig. 2e and f were SEM images of TiO_2 with an average particle size of 30 nm and 1 : 1.5 TiO_2/Ag_3PO_4 with a particle size less than 50 nm, respectively.

The main component of the hollow glass microspheres is soda lime borosilicate.[33] It can be clearly seen from Fig. 3 that the elements of HGMs-1 : 1.5 sample contained B, O, Na, Ca, Si originally contained in the HGMs. In addition, it also contained the C and N elements form the added APTES and the existence of Ti, Ag and P elements is verified. The EDS mapping qualitatively indicated that the particles supported on the HGMs contain Ti, Ag, and P elements, and the loadings of Ag and P elements were high.

The X-ray diffraction pattern of the raw material HGMs (Fig. 4a) has broad and weak diffraction peaks at 15–40°, but no characteristic diffraction peaks. The diffraction peak of TiO_2 (Fig. 4b) is the same as that of anatase TiO_2 in the JCPDS (No. 21-1272) standard spectrum library,[34] and the XRD pattern of HGMs–TiO_2 (Fig. 4c) shows the coexistence of HGMs and anatase TiO_2 diffraction phase, indicating the formation of HGMs–TiO_2 composites. The crystal sizes of the (101) diffraction peak of TiO_2 and HGMs–TiO_2 obtained from the Scherrer formula were 34.7 nm and 24.3 nm, which were in good agreement with the observation by SEM. The smaller particle size of TiO_2 supported on HGMs, in comparison with that of unsupported TiO_2, may be attributed to the pre-adsorption of Ti^{4+} onto the aminated HGMs surface *via* the electrostatic attraction with –NH_2 by lone pair of electrons to limit the growth of TiO_2 particles. The X-ray diffraction peak of pure Ag_3PO_4 (Fig. 4g) was matched with body-centered cubic Ag_3PO_4 crystal (JCPDS No. 06-0505).[35] As shown in Fig. 4h, the XRD spectrum contained all the characteristic diffraction peaks of Ag_3PO_4, but only contained a characteristic diffraction peak of the anatase TiO_2 (101) face, which might be due to the fact that TiO_2 was an inner layer coated with Ag_3PO_4, and the intensity of other characteristic diffraction peaks was weak. Therefore, the XRD pattern of 1 : 1.5 TiO_2/Ag_3PO_4 composite was basically expressed as the spectrum of Ag_3PO_4. The XRD patterns of

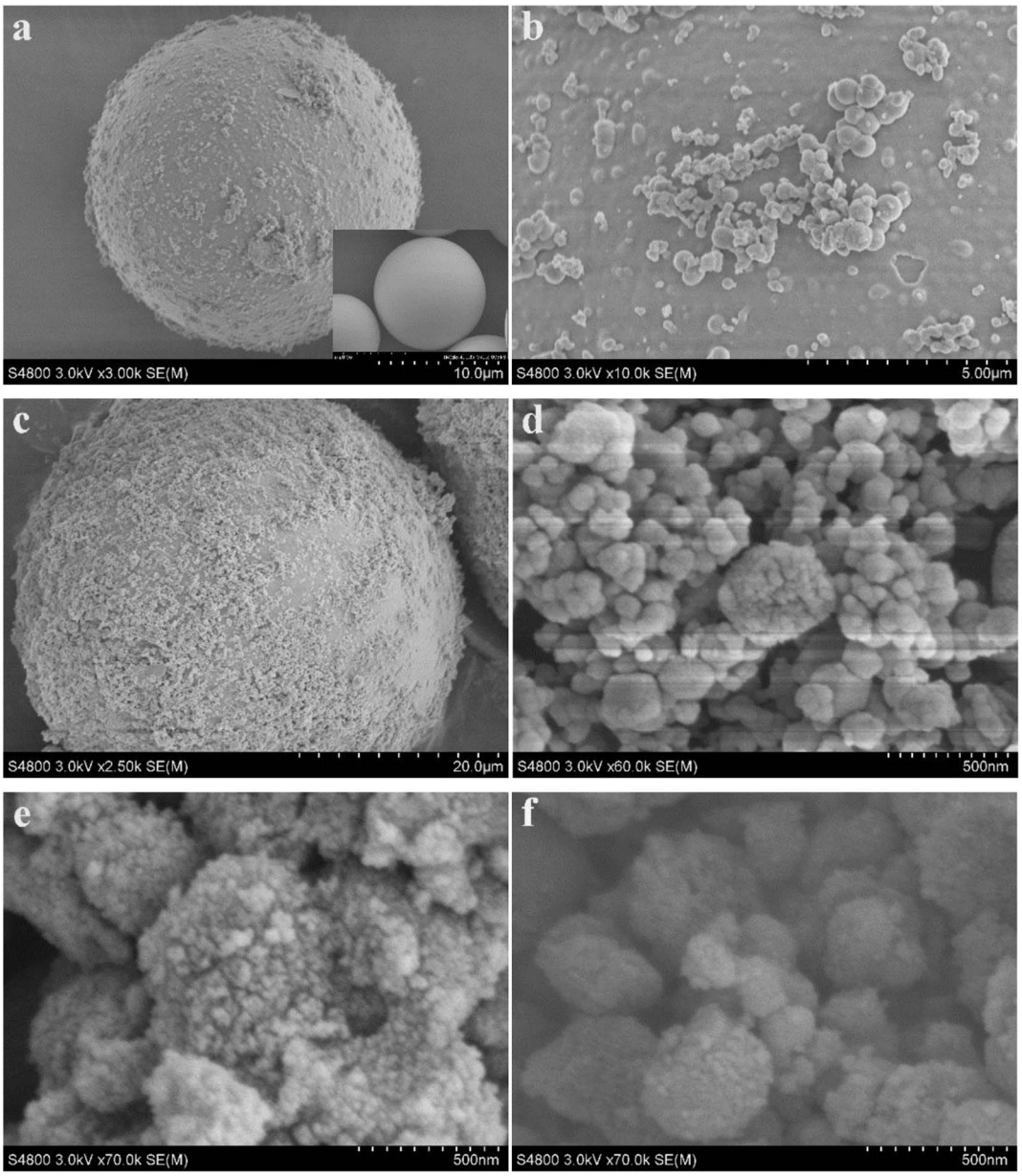

Fig. 2 SEM images of HGMs–TiO_2 (a and b), HGMs-1 : 1.5 (c and d), TiO_2 (e) and TiO_2/Ag_3PO_4 (f) inset: digital images of HGMs.

HGMs-1 : 1 (Fig. 4d), HGMs-1 : 1.5 (Fig. 4e) and HGMs-1 : 2 (Fig. 4f) show the coexistence of HGMs and Ag_3PO_4 diffraction phases, indicating that Ag_3PO_4 was loaded on the surface of HGMs. Compared with the XRD pattern of 1 : 1.5 TiO_2/Ag_3PO_4 composite (Fig. 4h), the TiO_2 diffraction peak was weaker and the diffraction peak of TiO_2 (101) plane in the three ratios of HGMs–TiO_2/Ag_3PO_4 composites could be covered by 15–40° wide diffraction peaks of the raw material HGMs. In summary, Ag_3PO_4 had been coated on the surface of HGMs–TiO_2.

The optical properties of HGMs, HGMs–TiO_2, TiO_2, HGMs–TiO_2/Ag_3PO_4 composites and pure Ag_3PO_4 were determined by UV-visible diffuse reflectance spectroscopy (Fig. 5). HGMs (Fig. 5a) had a certain UV absorption at wavelengths below 400 nm and almost no absorption in the visible wavelength range. Pure TiO_2 (Fig. 5c) absorbed ultraviolet light at wavelengths less than 385 nm, consistent with previous reports.[36] HGMs–TiO_2 (Fig. 5b) can absorb ultraviolet light less than 350 nm, which has a certain blue shift relative to TiO_2, which may be related to carrier HGMs. And pure Ag_3PO_4 (Fig. 5g) absorbed visible light less than 530 nm, which is equivalent to a band gap energy of 2.5 eV, in good agreement with the literature.[37] The three ratios of HGMs–TiO_2/Ag_3PO_4 composites (Fig. 5d, e and f) showed characteristic absorption peaks of pure TiO_2 in the ultraviolet wavelength range of less than 350 nm and a certain intensity absorption in the visible region, indicating the as-prepared HGMs–TiO_2/Ag_3PO_4 composites can be used for visible light photocatalytic reaction.

The actual Ag_3PO_4 loadings of HGMs–TiO_2/Ag_3PO_4 composites, including HGMs-1 : 1, HGMs-1 : 1.5 and HGMs-1 : 2, were determined by AAS and listed in Table 1. As the concentration of

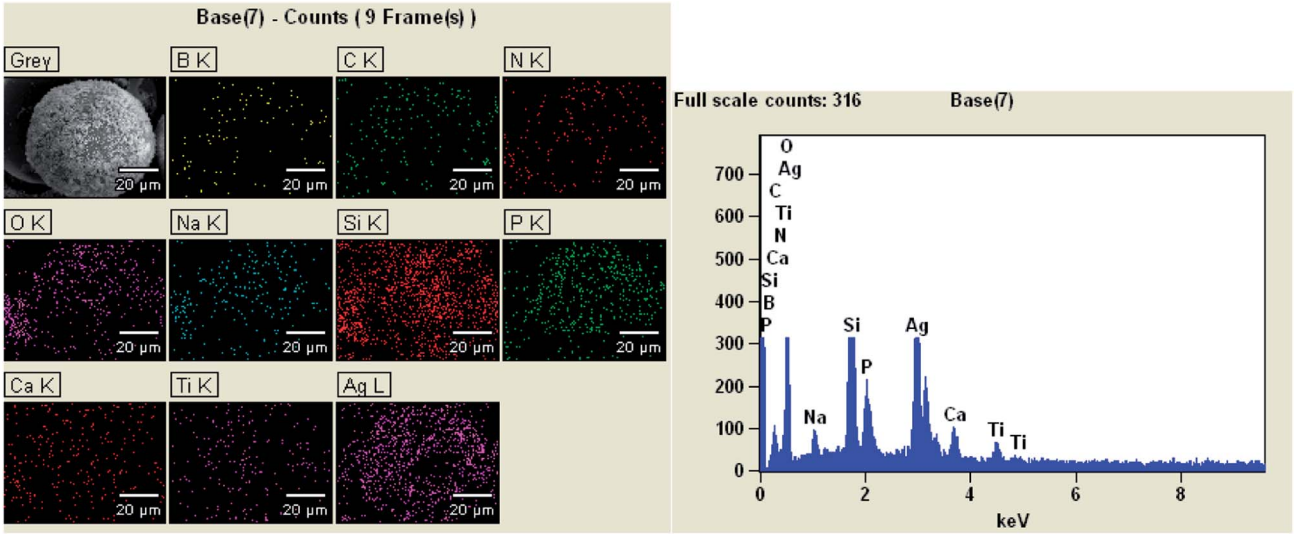

Fig. 3 EDS images of HGMs-1 : 1.5 sample.

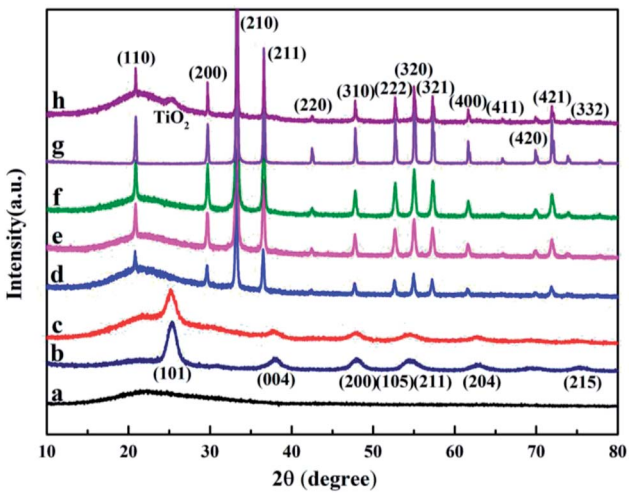

Fig. 4 X-ray diffraction patterns of HGMs (a), TiO_2 (b), HGMs–TiO_2 (c), HGMs-1 : 1 (d), HGMs-1 : 1.5 (e), HGMs-1 : 2 (f), pure Ag_3PO_4 (g) and 1 : 1.5 TiO_2/Ag_3PO_4 (h).

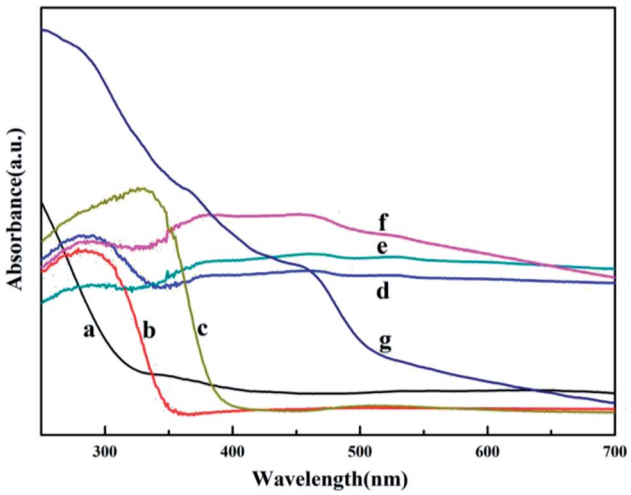

Fig. 5 UV-Vis diffuse reflectance spectra of HGMs (a), HGMs–TiO_2 (b), TiO_2 (c), HGMs-1 : 1 (d), HGMs-1 : 1.5 (e), HGMs-1 : 2 (f) and pure Ag_3PO_4 (g).

the reactants increased, the measured Ag_3PO_4 loading increased in the order of HGMs-1 : 1, HGMs-1 : 1.5, and HGMs-1 : 2. However, the actual load rate of Ag_3PO_4 decreased in turn and the degree of decline was not obvious. When TiO_2 was dispersed in silver nitrate solution, the negatively charged surface can adsorb Ag^+ to the surface by electrostatic attraction, which was beneficial to the increase of Ag_3PO_4 loading rate and form floating HGMs–TiO_2/Ag_3PO_4 composites. The loading ratios of the three proportional composites are similar, indicating that the titanium dioxide surface provides sufficient active sites to interact with Ag^+.

3.3. Photocatalytic properties for the degradation of methylene blue (MB) solutions

The effect of different ratios of TiO_2 and Ag_3PO_4 on the photocatalytic activity of floating HGMs–TiO_2/Ag_3PO_4 photocatalysts was compared by measuring the photodegradation rate of MB under visible light irradiation by simulating sunlight with a xenon lamp. The decolorization rate of MB as a function of time was shown in Fig. 6a. Taking the MB solution without any photocatalyst as a blank control, it can be seen from the figure that the MB solution is difficult to self-pyrolysis under illumination. Prior to illumination, the MB solutions containing raw material HGMs, different ratios of HGMs–TiO_2/Ag_3PO_4 composites, pure TiO_2 or Ag_3PO_4 or TiO_2/Ag_3PO_4 photocatalyst were placed in the dark for 60 min to achieve the adsorption–desorption equilibrium between the surface of photocatalysts and the MB. In the absence of irradiation, the decrease in the concentration of the MB solution was entirely attributable to the adsorption of the photocatalyst rather than the photodegradation. The raw material HGMs can adsorb about 8% of MB molecules result from the adsorption of dye cations by its surface Si–OH. TiO_2 and HGMs-1 : 0 almost completely adsorbed the MB in the solution without

Table 1 The Ag_3PO_4 loading on HGMs-1 : 1, HGMs-1 : 1.5, HGMs-1 : 2 determined by AAS

Samples	HGMs-1 : 1	HGMs-1 : 1.5	HGMs-1 : 2
The theoretical mass of Ag_3PO_4 loaded by per gram of HGMs per g	0.150	0.225	0.300
The theoretical mass of Ag^+ loaded by per 10 mg sample per mg	0.892	1.265	1.600
The measured mass of Ag^+ loaded by per 10 mg sample per mg	0.726	1.016	1.226
Actual load percentage	81.4%	80.3%	76.6%

illumination, because MB is a cationic dye and the negatively charged surface of TiO_2 can adsorb the positively charged MB^+ in the solution to the surface of TiO_2 by electrostatic attraction.[38] During the experiment, it was observed that the color of TiO_2 and HGMs-1 : 0 changed from the original white to blue. In addition, the TiO_2/Ag_3PO_4 photocatalyst could also adsorb nearly 80% of MB in the dark, which was also caused by the electrostatic adsorption of TiO_2. The percentages of MB adsorbed by HGMs-1 : 1, HGMs-1 : 1.5 and HGMs-1 : 2 samples in the dark were 35%, 39% and 48%, respectively, and their MB adsorption capacity enlarged with the increasing of Ag_3PO_4 ratios. After 90 min of exposure to visible light, the degradation of MB was as follows: HGMs-1 : 1.5 ≈ TiO_2/Ag_3PO_4 (96%) > HGMs-1 : 2 (92%) > HGMs-1 : 1 (86%) > Ag_3PO_4 (84%). For the floating HGMs–TiO_2/Ag_3PO_4 photocatalysts, the decolorization rate within 90 min was better than that of the single Ag_3PO_4 photocatalyst. The absorbance of the MB solution added with HGMs after the light was substantially unchanged, indicating that HGMs had no photocatalytic activity for MB. In addition, the floating characteristics of as-prepared HGMs-1 : 1.5 photocatalyst can be clearly seen from the inset of Fig. 6c, and the 5 mg L^{-1} MB solution could completely fade to a colorless solution after visible-light irradiation for 90 min, obviously indicating that HGMs-1 : 1.5 had excellent photocatalytic performance.

Kinetically, when the concentration of MB dye was very low, the kinetic properties of its photocatalytic degradation were in accordance with the Langmuir–Hinshelwood model, which expression is $\upsilon = -\frac{dC}{dt} = \frac{k_r KC}{1+KC}$.[39] In this formula, υ, k_r, K and C are the reaction rate, reaction rate constant, adsorption coefficient and the reactant concentration, respectively. When C is very small, $\upsilon \approx k_r KC = kC$ and $\ln\frac{C_0}{C} = kt$ is obtained. C_0 and C

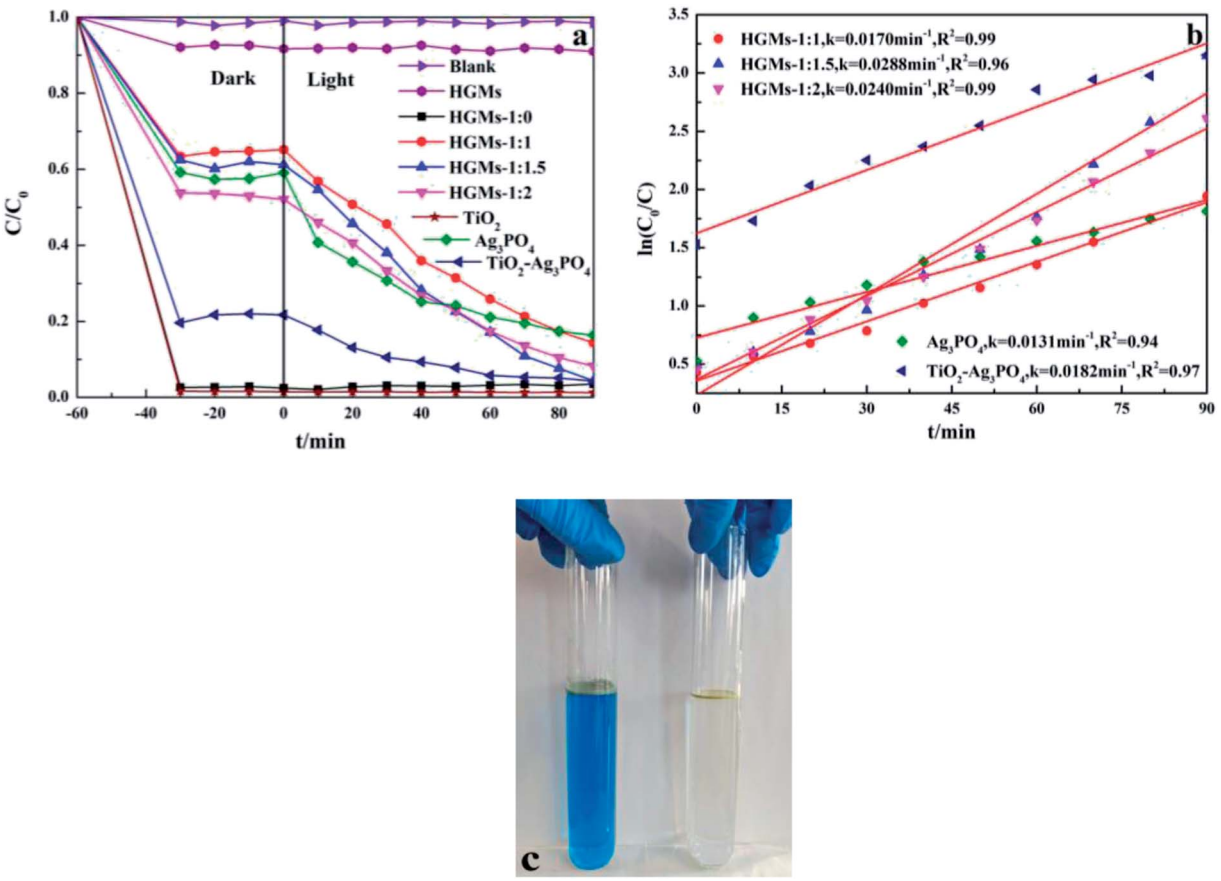

Fig. 6 (a) Photocatalytic degradation curve of 5 mg L^{-1} MB, (b) the kinetic fit of the MB degradation by 2 g L^{-1} HGMs-1 : 0, HGMs-1 : 1, HGMs-1 : 1.5, HGMs-1 : 2, pure Ag_3PO_4 and TiO_2/Ag_3PO_4, (c) digital picture of 60 mL 5 mg L^{-1} MB dye solution photo-catalytically degraded by 0.12 g HGMs-1 : 1.5 before (left) and after (right) 90 min of visible-light illumination.

are the concentrations of reactant at time 0 and t, and k is the apparent constant (first order rate). According to Beer–Lambert Law, C/C_0 is the ratio of the MB solution absorbance at each time interval to the absorbance of initial dye solution. The process of photocatalytic degradation of MB solution follows pseudo-first-order kinetic model. The photodegradation rate k is fitted by $\ln(C/C_0)$ *versus* t and the slope of the fitted line is the photocatalytic rate k, as shown in Fig. 6b. The apparent rate constant (k) for TiO_2/Ag_3PO_4 composite was 0.0182 min^{-1}, larger than that of single Ag_3PO_4 catalyst (k = 0.0131 min^{-1}). The k of HGMs-1 : 1, HGMs-1 : 1.5 and HGMs-1 : 2 were 0.0170 min^{-1}, 0.0288 min^{-1}, and 0.0240 min^{-1}, respectively. The HGMs-1 : 1.5 composite with a mass ratio of TiO_2 and Ag_3PO_4 of 1 : 1.5 had the highest rate constant k, which means this photocatalyst had the highest photocatalytic activity. While the Ag_3PO_4 content of floating HGMs-1 : 1.5 was less than pure Ag_3PO_4 and TiO_2/Ag_3PO_4, the photocatalytic properties were better than pure Ag_3PO_4 and TiO_2/Ag_3PO_4, which could be attributed to the larger light contact area.

The stability of the photocatalyst is one of the important parameters to measure its practicality. It is well-known that the Ag_3PO_4 photocatalyst is easily photo-etched under light conditions and reduced to Ag ($Ag^+ + e^- \rightarrow Ag^0$), which affects its photocatalytic activity. As shown in Fig. 7, after five consecutive cycles to degrade MB, Ag_3PO_4 almost lost its activity, while HGMs-1 : 1.5 still maintained a decolorization rate of about 75%, showing higher degradation efficiency and stability than pure Ag_3PO_4 and indicating that the presence of HGMs and the formation of heterostructure with TiO_2 were beneficial for improving photodegradation efficiency and stability of Ag_3PO_4. The floating HGMs–TiO_2/Ag_3PO_4 composites as a photocatalyst can not only greatly reduce the input of the Ag_3PO_4 catalyst and cost, but also significantly improve the photodegradation efficiency. In addition, it was easy to recycle in practical applications and had stable photocatalytic activity, indicating that the floating HGMs–TiO_2/Ag_3PO_4 composite can be used as an effective and promising visible light photocatalyst.

3.4. Possible mechanism of the improved photocatalytic activity

Several reasons may account for the enhanced photocatalytic activity of the floating HGMs–TiO_2/Ag_3PO_4 photocatalysts. Firstly, the HGMs-1 : 1.5 photocatalyst exhibited more enhanced visible light photocatalytic efficiency than that of pure Ag_3PO_4 and TiO_2/Ag_3PO_4 because HGMs-1 : 1.5 could float on the dye solution to enlarge the contact area with light, speeding up the excitation of visible light photons under the same test conditions. Secondly, with HGMs as the carrier, HGMs–TiO_2/Ag_3PO_4 composite can be uniformly dispersed on the surface of HGMs, which can not only enlarge the active surface area of the photocatalyst, but also increase lattice defects to generate new active centers, and improve its photocatalytic performance. Thirdly, Ag_3PO_4 itself had excellent photocatalytic performance due to the high dispersion of the conduction band (CB, + 0.45 V *vs.* NHE) and the large negative charge induction effect of PO_4.[3–40] However, with the prolongation of irradiation time, Ag_3PO_4 was easily reduced to Ag and Ag replaces active sites of original Ag_3PO_4, so the number both of photogenerated electrons (e^-) and holes (h^+) was reduced and the photocatalytic performance was degraded. The combination of Ag_3PO_4 and TiO_2 promoted the separation of e^- and h^+, and its photocatalytic activity was enhanced. The possible photocatalytic mechanism of HGMs–TiO_2/Ag_3PO_4 is depicted in Fig. 8. From the electron band structure of Ag_3PO_4 and TiO_2, the valence band (VB) potential of Ag_3PO_4 (+2.9 eV *vs.* NHE) is more positive than that of TiO_2 (+2.7 eV *vs.* NHE), and the conduction band potential of TiO_2 (−0.3 eV *vs.* NHE) is more negative than that of Ag_3PO_4 (+0.45 eV *vs.* NHE), which means that e^- and h^+ will be thermodynamically transferred to the CB of Ag_3PO_4 and the VB of TiO_2, respectively.[32,41–43] Under visible light irradiation, the e^- in the VB of Ag_3PO_4 absorbed energy from the photons (hv) to the CB and then further migrated to the surface of the Ag_3PO_4 particles, while h^+ was generated on the VB and rapidly transferred to the TiO_2 particles. The separation of e^- (in Ag_3PO_4) and h^+ (in TiO_2) prevents charge neutralization, and the

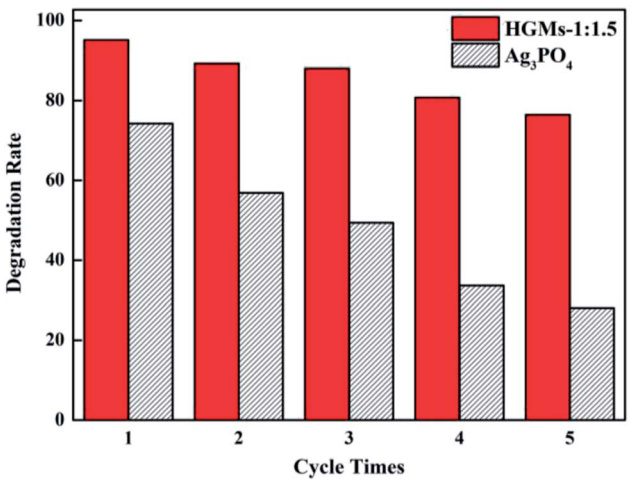

Fig. 7 Cycling runs of the 5 mg L^{-1} MB photo-degradation at the presence of 2 g L^{-1} HGMs-1 : 1.5.

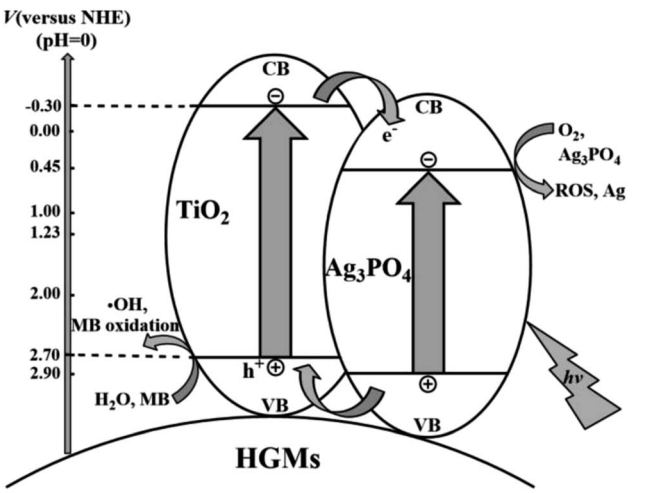

Fig. 8 Proposed mechanism for the MB photo-degradation of on the floating HGMs–TiO_2/Ag_3PO_4 composites.

close contact between the two semiconductor particles in the HGMs–TiO_2/Ag_3PO_4 composite promotes this interface charge transfer and separation, improving the photocatalytic activity. In addition, when the mass ratio of TiO_2 and Ag_3PO_4 was 1 : 1.5 among the three HGMs–TiO_2/Ag_3PO_4 samples, the photocatalytic activity of the sample reached an optimum value. When the content of Ag_3PO_4 exceeds this optimum value, the counteraction effect associated with e^- – h^+ recombination across TiO_2/Ag_3PO_4 interface may mediate carrier transfer to compromise the overall charge separation efficiency and lead to the depressed photocatalytic efficiency of type-II TiO_2/Ag_3PO_4 semiconductor heterostructures.[13] At the same time, the oxidizing h^+ in VB can directly oxidize the organic dye MB or indirectly oxidize MB by oxidizing H_2O molecules adsorbed to the surface of the photocatalyst to form strong oxidizing ·OH radicals[44,45] in that the VB level of TiO_2 is more positive than both 1.99 eV for OH^-/·OH and 2.37 eV for H_2O/·OH.[6] Furthermore, reducing e^- in CB can reduce the adsorbed O_2 molecules, and generate strong oxidizing reactive oxygen species (ROS, such as $\cdot O_2^-$, $HO_2^\bullet$, H_2O_2, ·OH, *etc.*) to oxidatively degrade MB. However, the redox potential of the ROS reaction (such as O_2/H_2O_2, +0.67 V) is similar to the potential of Ag_3PO_4/Ag (+0.45 V),[35] indicating that it will compete with the reduction reaction of Ag_3PO_4, so the photo-etching of Ag_3PO_4 semiconductor is still inevitable. Ag_3PO_4 are dispersed on the surface of HGMs to increase the active sites of photocatalytic reaction and the unique floating property of the photocatalyst enlarge the contact area of the HGMs–TiO_2/Ag_3PO_4 with light. Moreover, the combination of Ag_3PO_4 and TiO_2 on the surface of HGMs promotes the separation of photogenerated e^- and h^+, enhancing the photocatalytic performance and stability of the floating HGMs–TiO_2/Ag_3PO_4 composite.

4. Conclusions

In this work, the floating HGMs–TiO_2 was prepared by hydrothermal synthesis. Since TiO_2 only responded to ultraviolet light, Ag_3PO_4 was loaded into HGMs–TiO_2 composite by ion exchange method to form visible light-responsive floating HGMs–TiO_2/Ag_3PO_4 composites. The photocatalyst had the advantages of low density and high dispersion due to the use of micron-sized HGMs as a carrier, which made it float on the surface of the organic dye solution, enlarge the contact area with light and easy to recover. With MB as the photodegradation target, when the mass ratio of TiO_2 to TiO_2/Ag_3PO_4 is 1 : 1.5, the photocatalytic activity of the floating photocatalyst was better than that of pure Ag_3PO_4 and TiO_2/Ag_3PO_4, and its cycle stability was enhanced compared with single Ag_3PO_4. The floating HGMs–TiO_2/Ag_3PO_4 composites prepared by complexing TiO_2 with Ag_3PO_4 to form a heterojunction have potential application prospects in the photocatalyzed efficient degradation of organic pollutants under the visible-light irradiation, which greatly reduce the cost and enhance the photocatalytic performance.

Conflicts of interest

There are no conflicts to declare.

Acknowledgements

This research was supported by the National Nature Science Foundation of China (51462009, 51662011 and 21575100).

References

1 J. J. Blanco, S. Malato, P. Fernández-Ibañez, D. Alarcón, W. Gernjak and M. I. Maldonado, *Renewable Sustainable Energy Rev.*, 2009, **13**, 1437–1445.
2 J. M. Li, C. W. Tsao, M. J. Fang, C. C. Chen, C. W. Liu and Y. J. Hsu, *ACS Appl. Nano Mater.*, 2018, **1**(12), 6843–6853.
3 K. Nakata and A. Fujishima, *J. Photochem. Photobiol. C Photochem. Rev.*, 2012, **13**, 169–189.
4 S. Bagheri, Z. A. Mohd Hir, A. T. Yousefi and S. B. Abdul Hamid, *Microporous Mesoporous Mater.*, 2015, **218**, 206–222.
5 S. Bagheri and N. Muhd Julkapli, *Int. J. Hydrogen Energy*, 2016, **41**, 14652–14664.
6 Y. Duan, J. Luo, S. Zhou, X. Mao, M. W. Shah, F. Wang, Z. Chen and C. Wang, *Appl. Catal., B*, 2018, **234**, 206–212.
7 Y. H. Chiu and Y. J. Hsu, *Nano Energy*, 2017, **31**, 286–295.
8 Y. C. Pu, G. Wang, K. D. Chang, Y. Ling, Y. K. Lin, B. C. Fitzmorris, C. M. Liu, X. Lu, Y. Tong, J. Z. Zhang, Y. J. Hsu and Y. Li, *Nano Lett.*, 2013, **13**, 3817–3823.
9 Y. H. Chiu, T. H. Lai, C. Y. Chen, P. Y. Hsieh, K. Ozasa, M. Niinomi, K. Okada, T. M. Chang, N. Matsushita, M. Sone and Y. J. Hsu, *ACS Appl. Mater. Interfaces*, 2018, **10**, 22997–23008.
10 J. Guo, S. Ouyang, H. Zhou, T. Kako and J. Ye, *J. Phys. Chem. C*, 2013, **117**, 17716–17724.
11 B. Zhang, H. Zhang, Z. Wang, X. Zhang, X. Qin, Y. Dai, Y. Liu, P. Wang, Y. Li and B. Huang, *Appl. Catal., B*, 2017, **211**, 258–265.
12 H. Derikvandi and A. Nezamzadeh-Ejhieh, *J. Hazard. Mater.*, 2017, **321**, 629–638.
13 Y. S. Chang, M. Choi, M. Baek, P. Y. Hsieh, K. Yong and Y. J. Hsu, *Appl. Catal., B*, 2018, **225**, 379–385.
14 Y. F. Lin and Y. J. Hsu, *Appl. Catal., B*, 2013, **130–131**, 93–98.
15 B. Li, Y. Hao, B. Zhang, X. Shao and L. Hu, *Appl. Catal., A*, 2017, **531**, 1–12.
16 Y. C. Pu, W. H. Lin and Y. J Hsu, *Appl. Catal., B*, 2015, **163**, 343–351.
17 Z. Chen, Y. Ma, B. Geng, M. Wang and X. Sun, *J. Alloys Compd.*, 2017, **700**, 113–121.
18 F. Chen, W. An, L. Liu, Y. Liang and W. Cui, *Appl. Catal., B*, 2017, **217**, 65–80.
19 Q. Chen, Y. Wang, Y. Wang, X. Zhang, D. Duan and C. Fan, *J. Colloid Interface Sci.*, 2017, **491**, 238–245.
20 J. Feng, T. Chen, S. Liu, Q. Zhou, Y. Ren, Y. Lv and Z. Fan, *J. Colloid Interface Sci.*, 2016, **479**, 1–6.
21 H. Ramezanalizadeh and F. Manteghi, *J. Cleaner Prod.*, 2018, **172**, 2655–2666.
22 M. D. Hernández-Alonso, F. Fresno, S. Suárez and J. M. Coronado, *Energy Environ. Sci.*, 2009, **2**, 1231–1257.
23 M. Mousavi, A. Habibi-Yangjeh and M. Abitorabi, *J. Colloid Interface Sci.*, 2016, **480**, 218–231.

24 H. Yu, B. Huang, H. Wang, X. Yuan, L. Jiang, Z. Wu, J. Zhang and G. Zeng, *J. Colloid Interface Sci.*, 2018, **522**, 82–94.
25 M. Wu, J.-M. Yan, X.-W. Zhang, M. Zhao and Q. Jiang, *J. Mater. Chem. A*, 2015, **3**, 15710–15714.
26 X. Yao and X. Liu, *J. Hazard. Mater.*, 2014, **280**, 260–268.
27 Z. Yi, J. Ye, N. Kikugawa, T. Kako, S. Ouyang, H. Stuart-Williams, H. Yang, J. Cao, W. Luo, Z. Li, Y. Liu and R. L. Withers, *Nat. Mater.*, 2010, **9**, 559–564.
28 Y. Wang, B. Fugetsu, I. Sakata, W. Mao, M. Endo, M. Terrones and M. Dresselhaus, *Carbon*, 2017, **119**, 522–526.
29 W. Cao, Z. Gui, L. Chen, X. Zhu and Z. Qi, *Appl. Catal., B*, 2017, **200**, 681–689.
30 X. Yang, J. Qin, Y. Jiang, K. Chen, X. Yan, D. Zhang, R. Li and H. Tang, *Appl. Catal., B*, 2015, **166**, 231–240.
31 L. Luo, Y. Li, J. Hou and Y. Yang, *Appl. Surf. Sci.*, 2014, **319**, 332–338.
32 W. Yao, B. Zhang, C. Huang, C. Ma, X. Song and Q. Xu, *J. Mater. Chem.*, 2012, **22**, 4050–4055.
33 K. Zhao, H. Liu, T. Wang and H. Zeng, *J. Mater. Sci.: Mater. Electron.*, 2016, **27**, 5183–5189.
34 Y. Li, P. Wang, C. Huang, W. Yao, Q. Wu and Q. Xu, *Appl. Catal., B*, 2017, **205**, 489–497.
35 J. W. Xu, Z. D. Gao, K. Han, Y. Liu and Y. Y. Song, *ACS Appl. Mater. Interfaces*, 2014, **6**, 15122–15131.
36 L. Sun, S. Wan, Z. Yu and L. Wang, *Sep. Purif. Technol.*, 2014, **125**, 156–162.
37 J. Cao, B. Luo, H. Lin, B. Xu and S. Chen, *J. Hazard. Mater.*, 2012, **217–218**, 107–115.
38 R. Li, X. Song, Y. Huang, Y. Fang, M. Jia and W. Ma, *J. Mol. Catal. A: Chem.*, 2016, **421**, 57–65.
39 J. Ma, Q. Liu, L. Zhu, J. Zou, K. Wang, M. Yang and S. Komarneni, *Appl. Catal., B*, 2016, **182**, 26–32.
40 Y. Bi, S. Ouyang, N. Umezawa, J. Cao and J. Ye, *J. Am. Chem. Soc.*, 2011, **133**, 6490–6492.
41 M. Zhang, L. Li and X. Zhang, *RSC Adv.*, 2015, **5**, 29693–29697.
42 Y. Li, L. Yu, N. Li, W. Yan and X. Li, *J. Colloid Interface Sci.*, 2015, **450**, 246–253.
43 F. M. Zhao, L. Pan, S. Wang, Q. Deng, J. J. Zou, L. Wang and X. Zhang, *Appl. Surf. Sci.*, 2014, **317**, 833–838.
44 D. J. Martin, N. Umezawa, X. Chen, J. Ye and J. Tang, *Energy Environ. Sci.*, 2013, **6**, 3380–3386.
45 D. J. Martin, G. Liu, S. J. Moniz, Y. Bi, A. M. Beale, J. Ye and J. Tang, *Chem. Soc. Rev.*, 2015, **44**, 7808–7828.